Estimation of the Permeability Tensor of the Microvasculature of the Liver Through Fabric Tensors

Rodrigo Moreno, Patrick Segers, and Charlotte Debbaut

1 Introduction

Liver diseases represent a big burden for health systems. As an example, the prevalence of chronic liver conditions in Europe has been reported as high as 5.7% [1]. A full understanding of the circulatory system of the liver and how it is affected by different liver diseases can be used for designing better treatments. This knowledge can also be used in liver transplantation for both improving surgery planning and increasing the viability of the liver graft through hypothermic machine perfusion [6].

At the microscale, a promising procedure for studying the structure of the vasculature of the liver in vitro is to analyze vascular corrosion casts imaged through micro-computed tomography (micro-CT). At this scale, the liver is organized in functional units often referred to as lobules [9]. Blood flows in the lobule from vessels located at the corners towards the central vein in the center through microvessels called sinusoids. The boundaries of the lobules are referred to as vascular septa. Figure 1 shows a schematic representation of a lobule.

A strategy that has been followed by some researchers is to describe the lobules as a porous media which can be characterized through different parameters such as porosity, pore size, and permeability. Such models can be used to predict the microperfusion at a micro-level [2, 5].

R. Moreno (✉)
School of Technology and Health, KTH Royal Institute of Technology, Hälsovägen 11C, 14157 Huddinge, Stockholm, Sweden
e-mail: rodrigo.moreno@sth.kth.se

P. Segers • C. Debbaut
Biofluid, Tissue and Solid Mechanics for Medical Applications (bioMMeda), Institute Biomedical Technology (IBiTech), Ghent University, De Pintelaan 185, Block B, B-9000 Gent, Belgium
e-mail: patrick.segers@ugent.be; charlotte.debbaut@ugent.be

A. Wittek et al. (eds.), *Computational Biomechanics for Medicine*,
DOI 10.1007/978-3-319-54481-6_6

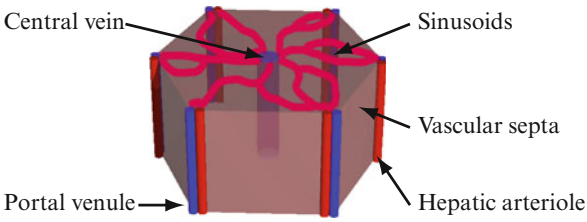

Fig. 1 Schematic representation of a liver lobule

One of the most important parameters in those models is the permeability, which measures how easy it is for a fluid to traverse a porous material. The discharge per unit area q (given in m/s) is related to the gradient of the pressure ∇p (given in Pa/m) in porous media through the Darcy's law:

$$q = \frac{-\mathsf{K}}{\mu}\nabla p, \tag{1}$$

where K is the permeability given in m^2 and μ is the dynamic viscosity given in Pa s. It is known that the permeability is not isotropic inside the lobules, which means that accurate models must consider second-order tensorial estimates of this parameter [4]. The permeability tensor is a symmetric positive definite second-order tensor, which can be represented by a 3×3 matrix. Basically, the permeability tensor depends on the geometry of the microvasculature, the properties of the vessel walls, the fluid dynamics properties of the blood, and properties of the parenchymal matrix.

Although it is possible to compute the permeability tensor through computational fluid dynamics (CFD) simulations in vascular corrosion casts imaged through micro-CT [4, 14], this approach has two main issues. On the one hand, the simulations require boundary conditions that are not straightforward to design. On the other hand, the computations are usually restricted to relatively small samples due to the expensive computational cost of the simulations. Thus, with this approach, the computation of the permeability tensor for a complete lobule usually requires averaging several permeability tensors computed from subsamples of the lobule.

CFD simulations require certain assumptions. It is well known that blood is a complex non-Newtonian fluid whose behavior varies depending on the diameter of the vessels. However, it is common to assume that blood behaves as a Newtonian fluid for computing the permeability tensor provided that the range of diameters of sinusoids inside the lobules is relatively reduced (8–20 μm) and blood flows at low velocities within those vessels. An important consequence of these assumptions is that the anisotropy and orientation of the permeability tensor mostly depends on the geometric arrangement of sinusoids of the lobule. This opens the door to approximating the permeability tensor through image processing-based methods for tackling the aforementioned issues of CFD simulations.

Fabric tensors are geometric features that describe the anisotropy and orientation of porous media [12]. In biomechanics, especially in trabecular bone research and material mechanics, fabric tensors have been used for two different purposes. First, different anisotropy measurements, e.g., fractional anisotropy (FA), can directly be extracted from tensors, which can potentially be used as quantitative imaging biomarkers. Second, fabric tensors can be combined with other parameters for predicting biomechanical tensors. For example, fabric tensors can be used for accurately estimating the stiffness tensor of trabecular bone in a few seconds [13]. Indeed, fabric tensors can also be applied to describe the microarchitecture of the microvessels in the lobules, considering that they can also be modeled as porous media. Although, the potential of this approach has recently been pointed out in [8], to the best of our knowledge, this is the first attempt of using fabric tensors in this context. Hence, the main aim of this paper is to explore the use of fabric tensors for approximating the permeability tensor of the liver lobules.

The paper is organized as follows. Section 2 describes the materials and methods. Section 3 compares the results with CFD. Finally Sect. 4 discusses the results and makes some concluding remarks.

2 Materials and Methods

2.1 Image Acquisition

A normal human liver which was discarded for transplantation after failed reallocation was used in this study.[1] A vascular corrosion cast was created for the liver using the standard procedure used in our lab [4]. First, a polymer resin was injected from the hepatic artery and portal vein to the liver until the resin reached the vena cava inferior. Second, the tissue surrounding the vessels was dissolved using potassium hydroxide.

Once the corrosion casts were obtained, a sample of size $1.1 \times 1.9 \times 1.5$ mm was taken for imaging through an in-house developed micro-CT scanner. The resolution of the images is $2.6\,\mu$m isotropic. This sample contains approximately three lobules of the liver, which were manually separated from each other. The images were segmented using Otsu's threshold. Vessels with diameters beyond $20\,\mu$m were discarded by just considering vessels that are filtered out by the opening operator of mathematical morphometry as described in [3, 10]. Figure 2 shows a rendering of the normal liver containing approximately three lobules.

[1]Ethical approval was obtained from the Ethical Committee of the University Hospitals Leuven (Belgium) and by the Belgian Liver and Intestine Committee.

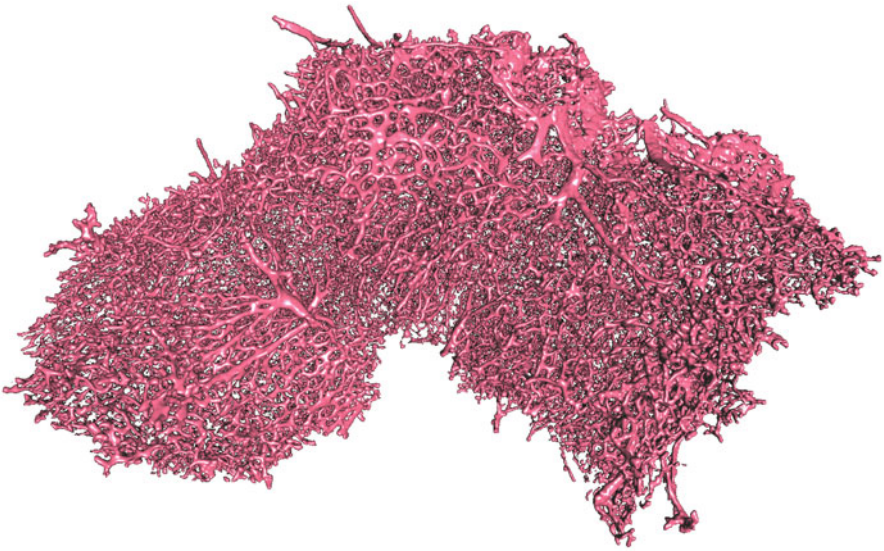

Fig. 2 Rendering of the micro-CT image of a sample taken from the normal liver containing three lobules

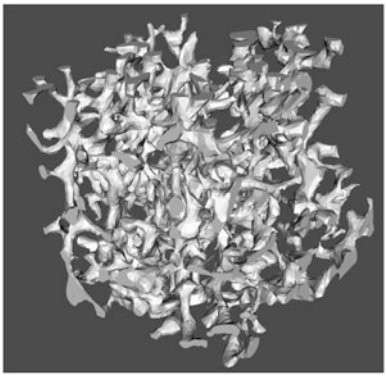

Fig. 3 Rendering of the section used for computing the permeability tensor through CFD

2.2 CFD Simulations

The CFD simulations were performed as described in [4]. A sample of 150 × 150 × 150 μm was cut from one of the three lobules. The z axis of the sample was aligned to the central vein. A surface mesh of the sample was used to create the volume meshes used in the simulations. Figure 3 shows the sample used for the CFD simulations.

Three simulations were performed, one per axis. In order to facilitate setting the boundary conditions for the simulations, two slabs of 15 μm were put perpendicular to the axis of interest before and after the sample in every simulation. A typical fluid

velocity was set at one slab and a zero pressure was set at the end of the opposite slab. CFD simulations were performed to estimate local velocities and pressures. By applying the Darcy's law, these values were used to compute the different entries of the permeability tensor for 15 subsamples of size $50 \times 50 \times 50\,\mu\text{m}$ taken from the original sample. Finally, these entries were averaged and the resulting tensors were symmetrized to get a single permeability tensor for the complete sample. A detailed description of the computations is given in [4].

2.3 Estimation of the Permeability Tensor Through Fabric Tensors

Methods for computing fabric tensors can roughly be classified into boundary- and volume-based [12]. Boundary-based fabric tensors have the advantage of being very efficient. From these, the generalized mean intercept length (GMIL) tensor [11] was chosen for this study since it has been proven versatile for predicting biomechanical tensors [13].

The GMIL tensor is computed in three steps. The mirrored extended Gaussian image (EGI) [7] is computed either from a robust estimation of the gradient or from a surface mesh. Second, the EGI is convolved with a kernel in order to obtain an orientation distribution function (ODF). Finally, a second-order fabric tensor is computed from the ODF. More formally, the generalized MIL tensor is computed as:

$$\mathsf{GMIL} = \int_{\Omega} \frac{v\, v^T}{C(v)}\, d\Omega\,, \tag{2}$$

where v are vectors on the unitary sphere Ω, and C is given by $C = H * E$: that is, the angular convolution $(*)$ of a kernel H with the mirrored EGI E. In particular, the von Mises–Fisher kernel, which is a function on the polar angle ϕ in spherical coordinates, is given by:

$$H(\phi) = \frac{\kappa}{4\pi \sinh(\kappa)}\, e^{\kappa \cos(\phi)}. \tag{3}$$

The advantage of using this kernel is that it has a parameter κ that can be used to control its smoothing action. A value of $\kappa = 8$ yielded the best results in the experiments of Sect. 3.

Fabric tensors are dimensionless descriptors, which means that they must be combined with other features for predicting the size of the permeability tensor. In this paper, we used the density of sinusoids ϵ for this purpose. In particular, we used a linear regression model between the Frobenius norm of the tensors obtained through CFD from the 15 subsamples used for computing the permeability tensor and their respective density $\epsilon (R^2 = 0.89)$.

3 Results

Figure 4 depicts the permeability tensor computed through CFD and fabric tensors. As shown, the shape of the two tensors is very similar and the main difference between them is their orientation.

Table 1 shows the eigenvalues of the two tensors before and after normalization as well as the FA.

The table shows that the shape of both tensors is very similar. Moreover, they tend to be orthotropic with respect to the central vein, which is consistent with the shape of the lobule shown in Fig. 1 and with the findings in [15]. Furthermore, the anisotropy in the axis parallel to the central vein is approximately twice the one in plane. Notice that the differences in the non-normalized eigenvalues are related to the linear model used to predict the size of the tensors and not with the use of fabric tensors.

The normalized difference of the norm D_N, the normalized difference of the FA D_{FA}, and the angle between the main eigenvectors D_A were computed to compare the permeability tensor computed through CFD and fabric tensors, which are referred to as $\mathsf{K}_{\mathrm{CFD}}$ and K_{FT}, respectively. These measurements are given by:

$$D_N = \frac{|\,||\mathsf{K}_{\mathrm{CFD}}||_F - ||\mathsf{K}_{\mathrm{FT}}||_F\,|}{||\mathsf{K}_{\mathrm{CFD}}||_F}, \tag{4}$$

$$D_{\mathrm{FA}} = \frac{|\mathrm{FA}(\mathsf{K}_{\mathrm{CFD}}) - \mathrm{FA}(\mathsf{K}_{\mathrm{FT}})|}{\mathrm{FA}(\mathsf{K}_{\mathrm{CFD}})}, \tag{5}$$

$$D_A = \arccos(|e1_{\mathrm{CFD}} \cdot e1_{\mathrm{FT}}|), \tag{6}$$

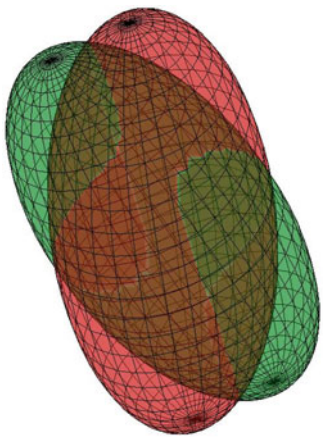

Fig. 4 Permeability tensor computed on a sample taken from a lobule. Results from CFD and fabric tensors are depicted in *green and red*, respectively

Table 1 Eigenvalues before and after normalization for a sample of a lobule

Tensor	λ_1 (f m^2)	λ_2 (f m^2)	λ_3 (f m^2)	λ_2/λ_1 (%)	λ_3/λ_1 (%)	FA (%)
K_{CFD}	32.01	17.26	14.27	53.91	44.56	42.12
K_{FT}	26.15	14.92	11.07	57.05	42.32	42.32

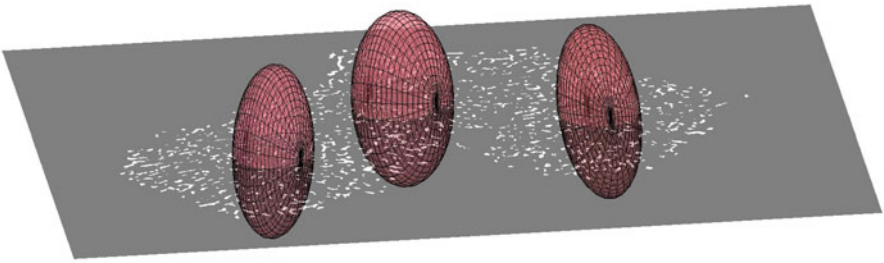

Fig. 5 Results for the three lobules. The tensors are plotted with a slice of the micro-CT image approximately where the central veins are located

Table 2 Eigenvalues after normalization for the complete lobules shown in Fig. 5

Lobule	λ_2/λ_1 (%)	λ_3/λ_1 (%)	FA (%)
Left	35.02	30.91	60.82
Center	31.40	25.21	66.69
Right	37.62	33.81	57.44

where $||\cdot||_F$ is the Frobenius norm, FA is the fractional anisotropy, and $e1$ is the eigenvalue corresponding to the largest eigenvalue of the tensor. These measurements are 17.9%, 0.2%, and 19.62° for the tested sample.

Figure 5 shows the results for the three lobules with the proposed method. As shown, the resulting tensors are approximately aligned with the orientation of the central veins. The corresponding CFD-based tensors were not available for comparison due to the high computational complexity of the simulations.

Table 2 shows the normalized eigenvalues and the FA for the three tensors. Similarly to the previous experiment, they exhibit orthotropic symmetry, but they have larger anisotropy.

As for computational effort, the new method took 330 ms for processing the result shown in Fig. 4 and 7.5 s per lobule for the results shown in Fig. 5. The CFD counterpart for Fig. 4 took several hours.

4 Discussion

A new method for estimating the permeability tensor of the microvasculature of the liver based on fabric tensors was presented. The main advantage of the new method is that it is very efficient and does not require to set boundary conditions. The results are promising, in particular with respect to the shape of the tensor, where the new method was able to reproduce the one obtained through CFD.

The results of this paper suggest that the permeability tensor is mostly related to the geometrical arrangement of the sinusoids. However, this finding must be validated with a larger dataset. Actually, the main limitation of this study is that,

due to ethical restrictions, it is difficult to have access to more data. One way to circumvent this problem is to work with animal models, something that will be tested in our lab.

Additional ongoing research include improving the estimation of the size of the tensors and improving the CFD simulations in order to consider the non-linear dependency of the permeability tensor on the gradient of the pressure as reported in [16].

References

1. Blachier M, Leleu H, Peck-Radosavljevic M, Valla DC, Roudot-Thoraval F (2013) The burden of liver disease in Europe. J Hepatol 58:593–608
2. Bonfiglio A, Leungchavaphongse K, Repetto R, Siggers JH (2010) Mathematical modeling of the circulation in the liver lobule. J Biomech Eng 132(11):111011
3. Coeurjolly D (2010) Fast and accurate approximation of the Euclidean opening function in arbitrary dimension. In: IEEE International Conference on Pattern Recognition (ICPR), pp 229–232
4. Debbaut C, Vierendeels J, Casteleyn C, Cornillie P, Van Loo D, Simoens P, Van Hoorebeke L, Monbaliu D, Segers P (2012) Perfusion characteristics of the human hepatic microcirculation based on three-dimensional reconstructions and computational fluid dynamic analysis. J Biomech Eng 134(1):011003
5. Debbaut C, Vierendeels J, Siggers JH, Repetto R, Monbaliu D, Segers P (2014) A 3D porous media liver lobule model: the importance of vascular septa and anisotropic permeability for homogeneous perfusion. Comput Methods Biomech Biomed Eng 17(12):1295–1310
6. Debbaut C, Monbaliu DRL, Segers P (2014) Validation and calibration of an electrical analog model of human liver perfusion based on hypothermic machine perfusion experiments. Int J Artif Organs 37(6):486–498
7. Horn BKP (1984) Extended Gaussian images. Proc IEEE 72(12):1671–1686
8. Jiřík M, Tonar Z, Králíčková A, Eberlová L, Mírka H, Kochová P, Gregor T, Hošek P, Svobodová M, Rohan E et al (2016) Stereological quantification of microvessels using semiautomated evaluation of X-ray microtomography of hepatic vascular corrosion casts. Int J Comput Assist Radiol Surg 11(10):1803–1819
9. Marieb EN, Hoehn K (2008) Anatomy & physiology. Pearson Education, San Francisco
10. Moreno R, Borga M, Smedby Ö (2012) Estimation of trabecular thickness in gray-scale images through granulometric analysis. In: Proceedings of SPIE. Medical Imaging 2012: Image Processing, vol 8314, p 831451
11. Moreno R, Borga M, Smedby Ö (2012) Generalizing the mean intercept length tensor for gray-level images. Med Phys 39(7):4599–4612
12. Moreno R, Borga M, Smedby Ö (2014) Techniques for computing fabric tensors: a review. In: Westin CF, Vilanova A, Burgeth B (eds) Visualization and processing of tensors and higher order descriptors for multi-valued data. Springer, Berlin, pp 271–292
13. Moreno R, Smedby Ö, Pahr DH (2016) Prediction of apparent trabecular bone stiffness through fourth-order fabric tensors. Biomech Model Mechanobiol 15(4):831–844
14. Peeters G, Debbaut C, Cornillie P, De Schryver T, Monbaliu D, Laleman W, Segers P (2015) A multilevel modeling framework to study hepatic perfusion characteristics in case of liver cirrhosis. J Biomech Eng 137(5):051007

15. Ricken T, Dahmen U, Dirsch O (2010) A biphasic model for sinusoidal liver perfusion remodeling after outflow obstruction. Biomech Model Mechanobiol 9(4):435–450
16. Rohan E, Lukeš V (2015) Modeling nonlinear phenomena in deforming fluid-saturated porous media using homogenization and sensitivity analysis concepts. Appl Math Comput 267:583–595